J Ther Eng, Vol. 12, No. 2, pp. 814−826, March, 2026

Journal of Thermal Engineering
Web page info: https://jten.yildiz.edu.tr
DOI: 10.14744/thermal.0001120

Research Article

The development and evaluation of a solar Stirling engine integrated with an annular Fresnel lens concentrator system

Yasir MEHMOOD[1], Asnaf AZIZ[1], Abid HUSSAIN[1,*], Fasih Ur RAHMAN[1], Afzal KHAN[1], Muhammad ABUBAKKAR[1], Imad RASOOL[1]

[1]Department of Mechanical Engineering, University of Engineering and Technology Peshawar, 25120, Pakistan

ARTICLE INFO

Article history
Received: 22 October 2024
Revised: 26 December 2024
Accepted: 08 January 2025

Keywords:
Alpha Configuration; Clean Energy; Computational Modelling; Heat Exchanger Design; Solar Concentrator; Solar Energy; Stirling Cycle; Stirling Engine

ABSTRACT

The study addresses the critical energy and environmental crises by exploring renewable energy sources, with a focus on solar energy. Solar Stirling engines are particularly relevant due to their efficiency in converting solar energy into electricity. This research presents the development and evaluation of a solar Stirling engine integrated with an annular Fresnel lens concentrator system. Designed to operate within a temperature range of 370–450 °C with air as the working fluid, the engine's performance was assessed by measuring pressure drops in the regenerator and energy losses in the cylinders. Experimental results revealed that the alpha configuration prototype produced 37 watts of power with an efficiency of 26.4%. These findings underscore the engine's effectiveness in solar energy conversion and its potential for practical applications in generating electricity. The integration of the Fresnel lens concentrator represents a novel approach not extensively covered in existing literature. The study's optimization of the engine's design and detailed performance metrics contribute to improved efficiency and broader applicability of solar Stirling engines, offering a viable solution for reducing reliance on fossil fuels and addressing environmental challenges.

Cite this article as: Mehmood Y, Aziz A, Hussain A, Rahman FU, Khan A, Abubakkar M, Rasool I. The development and evaluation of a solar Stirling engine integrated with an annular Fresnel lens concentrator system. J Ther Eng 2026;12(2):814−826.

INTRODUCTION

Increased energy demands have led to both an energy crisis and an environmental crisis [1]. More than ever, renewable alternatives are needed to address the energy and environmental problems. One major reason the world is turning towards renewable resources is the fast-growing environmental degradation. Climate change is causing havoc everywhere, from melting glaciers and rising sea levels to historical rains, storms, and subsequent floods. Carbon emissions are major constituent of global warming. According to the EIA (US Energy Information Administration), CO_2 emissions by fuel generation are 2.38 and 2.30 pounds per kWH, respectively, for petroleum and coal [2]. Solar energy, harnessed from the Sun, is a viable and diverse energy source, encompassing both direct and indirect applications. The Earth's surface

***Corresponding author.**
*E-mail address: abidhussain@uetpeshawar.edu.pk

This paper was recommended for publication in revised form by Editor-in Chief Ahmet Selim Dalkilic

receives approximately 60% of the total solar energy that reaches our planet. Despite this substantial influx, only about 0.1% of this solar energy is currently converted into usable forms, reflecting a significant potential for expansion. In terms of capacity, the theoretical maximum energy generation from solar power is estimated to be around 5000 gigawatts (GW) if fully exploited. This highlights the immense potential of solar energy compared to current energy production levels [3]. The primary method of converting solar energy is through Solar Photovoltaic (SPV) systems, which directly convert sunlight into electricity. In addition to SPV systems, another key technology is Solar Thermal Systems (STS). STS focus on converting solar energy into heat, which can then be used for a variety of heating and cooling applications. This heat can be employed for tasks such as space heating, water heating, and cooling processes, making STS a versatile and important technology for harnessing solar energy [4]. Meanwhile, all other energy sources have carbon emissions of 0.86 pounds per kWH. That's around 270% less than fossil fuels. According to another study by Guidi G et al. [5], in comparison to fossil fuel technologies, all of the emission estimates found for renewable energy sources are lower by at least one order of magnitude, sometimes even two orders of magnitude. Hydroelectricity and wind power are promising, but location and expense limit their application. This makes solar energy more easily accessible and usable in widespread applications. Solar energy thrives in isolated deserts, but photovoltaic cells struggle under severe temperatures. In contrast, solar Stirling engines transform solar energy into electricity efficiently. Stirling engine is a type of external combustion engine developed by Robert Stirling in 1816. The Stirling engine undergoes the four fundamental stages of compression, heating, expansion, and cooling, just like any other heat engine. Any heat source, including solar, geothermal, nuclear, and waste heat from industrial processes, can be used to power a Stirling engine directly. As solar energy is excessively available and comparatively easy to harness, solar Stirling engines are favorable to be used to produce electricity. Air is initially compressed in this engine utilizing work, that has been accumulated from a previous cycle in the mechanical flywheel. Different temperatures are applied to the working fluid to transform the whole amount of heat energy into mechanical work. Thermal equilibrium is present for the working fluid. The ability of this engine to run with any heat source is by far its greatest benefit. These engines are appropriate for solar energy that is concentrated and renewable [6].

Stirling engines are simplistic and highly efficient in their design, with theoretical efficiency almost equal to the Carnot efficiency [6]. This makes them a good choice for generating power from different heat sources, even from waste heat in industries such as cement plants. Solar Stirling engines are also advantageous over solar photovoltaic arrays as their solar-to-electric power conversion is more efficient [7]. Hence, in environments such as deserts and urban areas, which have high summertime temperatures, stirling engines can be used for efficient power production. In the 1870s, Ericsson constructed the inaugural "Sun Engine", a Solar Stirling engine that harnessed a parabolic mirror to convert heat into steam, which functioned as the operational fluid for the engine. Following the invention of internal combustion engines, the progress in the development of sterling engines diminished, and they were subsequently only utilized for certain applications, such as in submarines.

Recently, there has been a global shift towards renewable energy sources and an increased exploration of alternative methods for power generation. The resurgence of Solar Sterling Engines has prompted academics to examine and investigate their utilization in various situations and arrangements. In the early 2000s, joint research was done on the production of a parabolic dish solar Stirling engine called EnviroDish [8]. Cinar, C., and H. Karabulut manufactured and studied a gamma-type Stirling engine. With experimental results, they concluded that the use of Helium gas as a working fluid resulted in more power than air and hydrogen [9]. In the dynamic analysis of a GPU-3 model, researchers discovered that geometrical and physical parameters significantly impact its performance. Through optimization techniques, they successfully reduced mechanical losses and achieved more realistic theoretical outcomes [10].

Regenerator materials with various porosities suggest that the stainlesssteel regenerator with 85% porosity gave optimum results [11]. A. Nielsen et al. [12], did a study that showed that using a multistage regenerator increases the efficiency of the regenerator in comparison to a single-stage regenerator. A recent study was performed regarding the construction and testing of a dish-type solar Stirling engine and the losses in the solar-to-electric conversion. This study found that the dish reflector should not concentrate the sun's rays onto a point of the Stirling engine but rather a zone [13]. Abuelyamen et al. [13], conducted an in-depth CFD analysis to assess the energy efficiency of different types of Stirling engines, (α, β, and γ). The use of solar power Stirling engines in marine and offshore environments also bear great potential: a study shows the solar power Stirling engine system achieved a maximum of 90% mechanical efficiency [14]. Bataineh did a study on the numerical thermodynamic model of the solar sterling engine and discussed Kinetic and thermodynamic parameters of the engine [15].

However, one area of research yet to be fully explored is the application of an annular Fresnel lens system paired with an alpha configuration sterling engine for power production, as most of the research has been focused on the use of parabolic dish concentrators. Heng Zheng et al. [16], did a study on a solar-aided power generation system that used an annular frequency solar. Similarly, a study was done by Boretti that shows the use of an annular concentrator for power production application [17]. An advantage of the Alpha Stirling engine is its ability to include a regenerator in its design easily. The regenerator can occupy the dead space that links the hot and cold cylinders, enhancing the engine's efficiency.

Meanwhile, the beta configuration has a single-cylinder design that places hot and cold cylinders in close proximity. Moreover, for our specific temperature range and simplicity with manufacturing alpha configuration was more feasible.

Solar Stirling engines can be utilized in isolated areas to provide off-grid power. Their capacity to transform solar energy into electricity makes them excellent for rural or remote places where traditional power infrastructure is limited [18]. In urban or suburban areas, these engines can be linked into local energy systems to augment the grid, resulting in a more sustainable and robust energy network [19]. The Alpha Stirling engine's design innovations allow for a wide range of uses, including energy generation, industrial use, and education. The findings highlight its potential to improve efficiency and sustainability, meeting the different needs of the journal's readership while also contributing to broader discussions on renewable energy and technological innovation [20]. Recent studies have focused on improving the efficiency of Stirling engines by optimizing materials and thermal management. A study published in Energy Storage and Technology explores advanced heat exchangers and novel materials for Stirling engines, highlighting improvements in thermal efficiency and reducing mechanical losses. This work complements the findings of this paper by emphasizing the importance of material selection in enhancing the performance of Stirling engines [21].

The paper details developing and evaluating a solar Stirling engine utilizing an annular Fresnel lens concentrator system for generating power. The system's characteristics were chosen based on a temperature range of 370–450 °C during the design phase, with air being used as the working fluid. The system is examined via dynamic models to assess pressure drop in the regenerator and energy losses in the cylinders. With a robust design, the system is engineered for maximum output and efficiency. The engine's thermodynamic and mechanical parameters are also calculated and examined. Experimental tests are conducted on a prototype design utilizing an alpha configuration, resulting in 37W of output work with an efficiency of 26.4%.

MATERIALS AND METHODS

The Stirling engine model was designed according to design parameter calculations with the help of design software such as SolidWorks, and computations were done with the help of ANSYS. The selection of engine type and configuration was based on the study objectives and market limitations. After careful iterative measures, an alpha-type Stirling with a 90-degree V-configuration was selected, and an annular Fresnel lens concentrator was also designed as per similar criteria. Design considerations included selecting the material and geometry to optimize solar radiation collection and incorporating heat transfer enhancements. Factors such as thermal conductivity, specific heat capacity, and stability at high temperatures were taken into account. Paetro analysis was performed using software to select the optimum design parameters. The selection is based on efficiency, cost, safety, and environmental impact. Optimizing surface area, fluid flow pathways, and heat transfer coefficients are also considered. Thermodynamic and kinematic safety analysis of the system design were performed using ANSYS and MATLAB, whereas characteristic equations were solved with the help of Mathcad software. An approach similar to Aigboviosa et al. [22], 2018 was used where we programmed two motors for solar tracking for optimum solar irradiance.

Designing components such as pistons, cylinders, cranks, etc. involved taking material choice, stress analysis, and friction reduction into account. A feedforward control system was utilized to preserve optimal SSE functioning and maximize efficiency. Computer simulations and analytic tools were utilized throughout the design phase to assess system performance, forecast energy production, and optimize design parameters.

The design methodology frequently employed for designing a Stirling engine involves an iterative design process aimed at achieving the most optimal design conclusion shown in figure 1. A basic conceptual design is made by selecting the key features, such as an estimate of power output, temperature range type of mechanism used. This methodology comprises two analysis procedures: Schmidt analysis and non-dimensional analysis. Initial values are estimated, and the iteration is carried out for optimum design parameters such as piston size, etc.

The receiver absorbs concentrated solar energy and transfers it to a working fluid to heat it. A Fresnel lens concentrator system focuses sunlight on a focal point that contains the working fluid and serves as the receiver. The cycle starts with the high-temperature cylinder in its highest position. As the gas heats up, it expands, pushing the piston downward. This is the power piston. The sealed chamber in which the heated working fluid is housed expands as the heat energy is absorbed. This expansion transforms the heat energy into mechanical work by propelling the piston. After developing, the working fluid is sent to a heat exchanger or cooling mechanism, where it releases heat to the surroundings, through air. The working fluid's temperature is reduced over this cooling process. After cooling, the low-temperature piston displaces the gas back into the regenerator. The regenerator now releases heat stored earlier into the working gas. And the gas goes back to the hot cylinder, and the cycle repeats.

A steel mesh regenerator was utilized, consisting of a hollow mild steel exterior body filled with stainless steel mesh. Because regenerator efficiency depends on surface area, a mesh was employed instead of a solid body. Furthermore, as Geith et al. demonstrated in their study, stainless steel is 30% more thermally efficient than copper and aluminum, both of which have temperature and oxidation restrictions. The characteristics and materials were chosen based on prior research by Geith, Timoumi, and others that examined the impacts of pressure drop, thermal conductivity, and thermal capacity.

Materials were chosen based on their thermal conductivity, specific heat capacity, and stability at high temperatures to ensure effective heat transfer and structural integrity. High-performance materials with excellent thermal conductivity were selected for components in direct contact with the working fluid to enhance heat transfer. Additionally, materials with high specific heat capacity were used to ensure that the engine could efficiently store and release thermal energy. In the Stirling engine, heat transfer enhancements included the optimization of surface area and fluid flow pathways, as well as the implementation of advanced heat exchangers and regenerative systems to improve overall thermal efficiency. The materials used is aluminum alloy t6061 for the cylinder and hot source whereas the cylinder sleeve is made up of cast iron.

The laser temperature gun with specifications, (Temperature Range -60°C -800 °C), dynamometer and tacheometer (Range 0.5 ... 19999 rpm, Resolution 0.5 rpm (< 1000 rpm) 1 rpm (>1000 rpm) in the studies were used.

The Cycle consists of cyclic isothermal expansion and compression with an isochoric regeneration process as shown in figure 2. In the figure from processes 1-2, we have an isothermal or constant temperature compression, and then from 2-3, we have a constant volume increase in pressure. Then from 3-4, we have isothermal volume change or constant temperature expansion. Then, from 4-1, we again have a constant volume process. From 1-4 to 2-3, we have an isochoric regeneration process where a part of the heat from the earlier process is retained at the regenerator and is then added to the next process from the cold region, making it more efficient [23].

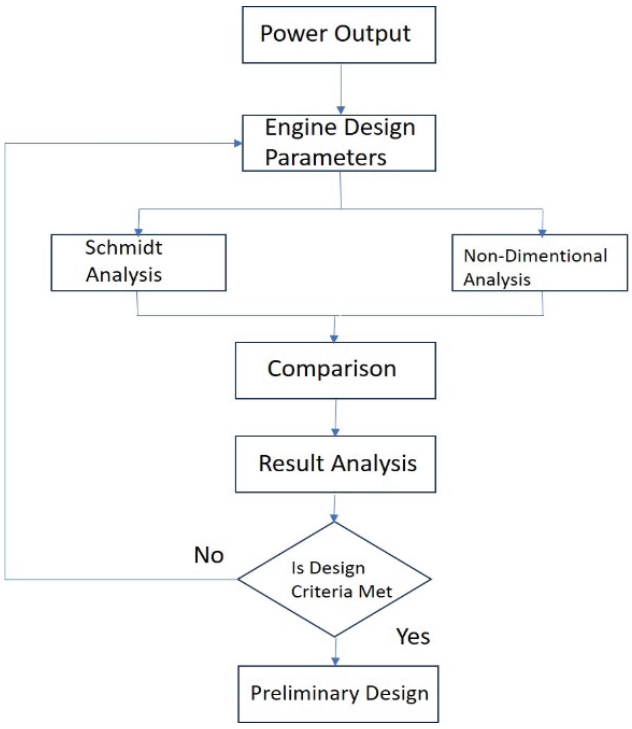

Figure 1. Flowchart for design of Stirling engine.

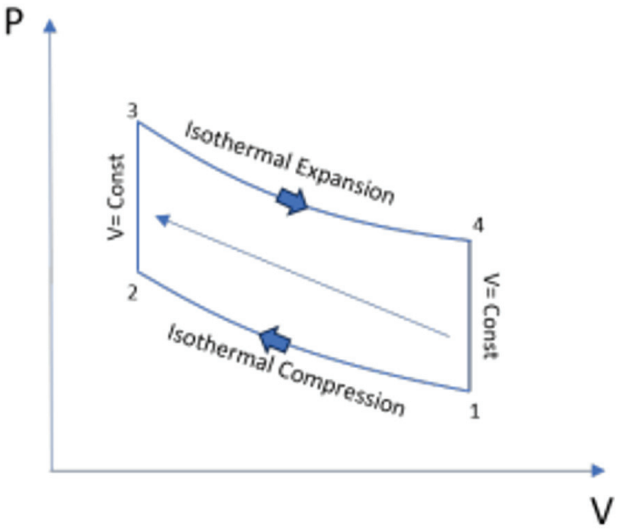

Figure 2. Stirling Cycle Process Diagram [23] [Open accessed].

RESULTS AND DISCUSSION

The Stirling engine comprises three essential components: the hot chamber, the cold chamber, and the regenerator, as shown in figure 4. The hot chamber interfaces with a heat source, while the cold chamber interacts with a heat sink. Gas seamlessly flows between these chambers via the regenerator. The power piston generates mechanical work, while the displacer piston orchestrates the movement of gas between chambers, instigating oscillations in temperature and pressure that propel the power piston. The engine's parameterization employed MATLAB's iterative hit-and-trial method, selecting 70-cc pistons with a 47-mm bore diameter and refining the volumes of the displacement and power pistons through successive MATLAB trials. The dimension and Specifications of alpha Stirling engine are given in Table 1. The nomenclature of Stirling engine is given in Table 2 and the important calculations are given in Table 3.

Table 1. Stirling Engine Cycle

Stirling Engine	Dimensions& Specifications
Height	243 mm
Length	237 mm
Width	184 mm
Mass	11 kg
Displacer Piston	47 mm
Power Piston	47 mm
Stroke	56 mm
Working Gas	He / Air

Table 2. Nomenclature

Symbol	Quantity	Units
P_{engine}	Operating Pressure in Engine	bar
V_{exp}	Total Expansion volume in the pistons	mm^3
V_{comp}	Total Compression Volume in the piston	mm^3
V_{se}	Expansion Swept Volume	mm^3
V_{de}	Expansion Dead Volume	mm^3
V_{sc}	Compression Piston Swept Volume	mm^3
V_{dc}	Compression piston Dead Volume	mm^3
P	Preload Pressure	bar
W_{exp}	Work done by expansion pistons	J
W_{comp}	Work done by compression Pistons	J
L	Length of the connecting rod	mm
r	Crank radius	mm
α	Slider crank acceleration	m/s^2
v	Slider crank velocity	m/s
x	Slider crank displacement	m
ω	Angular velocity of the engine, at 1000 rpm	Rad/s
θ	Crank angle	deg
m_b	Combined mass of slider crank	g
T	Torque produced in the engine	Nm
σt_{max}	Maximum stress in the flywheel	MPa
η_{ly}	Flywheel efficiency	No unit

According to Schmidt analysis [24] the work done by the engine is calculated as

$$P_{engine} = \frac{P.\sqrt{1-c^2}}{1-c.\cos(\Theta-\alpha)} \tag{1}$$

Here Pengine [25]gives the total Pressure in the engine with the crank angle θ, having initial engine pressure that was provided to the gas before the engine is started.

$$V_{exp} = \frac{V_{se}}{2}(1-\cos\Theta) + V_{de} \tag{2}$$

$$V_{comp} = \frac{V_{sc}}{2}(1-\cos\Theta - dx) + V_{dc} \tag{3}$$

From the Schmidt analysis [24], the work done by the engine is given by,

$$W_{exp} = \frac{P.V_{se}.\pi.c.\sin a}{1+\sqrt{1-c^2}}$$
$$W_{exp} = 61.642\ J \tag{4}$$

Figure 5 shows the Stirling Engine's characteristics. Figure 5a, presents the pressure vs. volume graph. The area under the graph gives us the total work done by the engine.

Table 3. Stirling Engine Calculations

Symbol	Quantity	Value	Unit
V_1	Hot Swept Volume of Displacer	1.9431×10^5	mm^3
V_p	Cold Swept Volume of Power-Piston	1.9431×10^5	mm^3
V_h	Hot Dead Volume of Displacer Piston	91000	mm^3
V_c	Cold Dead Volume of Power Piston	50000	mm^3
V_r	Regenerator Dead Volume	182500	mm^3
R	Specific gas Constant	287.1	J/Kg K
P	Preload Pressure in System	7	bar
T	Highest Temperature of System	673	K
T_c	Compression Space Gas Temperature	303	K
T_r	Regenerator Temperature	463.6519	K
M	Mass of Gas in System when the Slider-Crank is at an angle of 0	21.7568	10^{-1} g
S	S	3.5529	
B	Beale Number	1.0967	
C	C	0.3087	
P_m	Mean Pressure	5.7645	Bar
a_1	a_1	65.7616	degree
W_e	Work done by expansion piston	61.642	J
W_c	Work done by Compression piston	27.739	J
W_i	Total Work	34.263	J
	Compression Ratio	2.2	

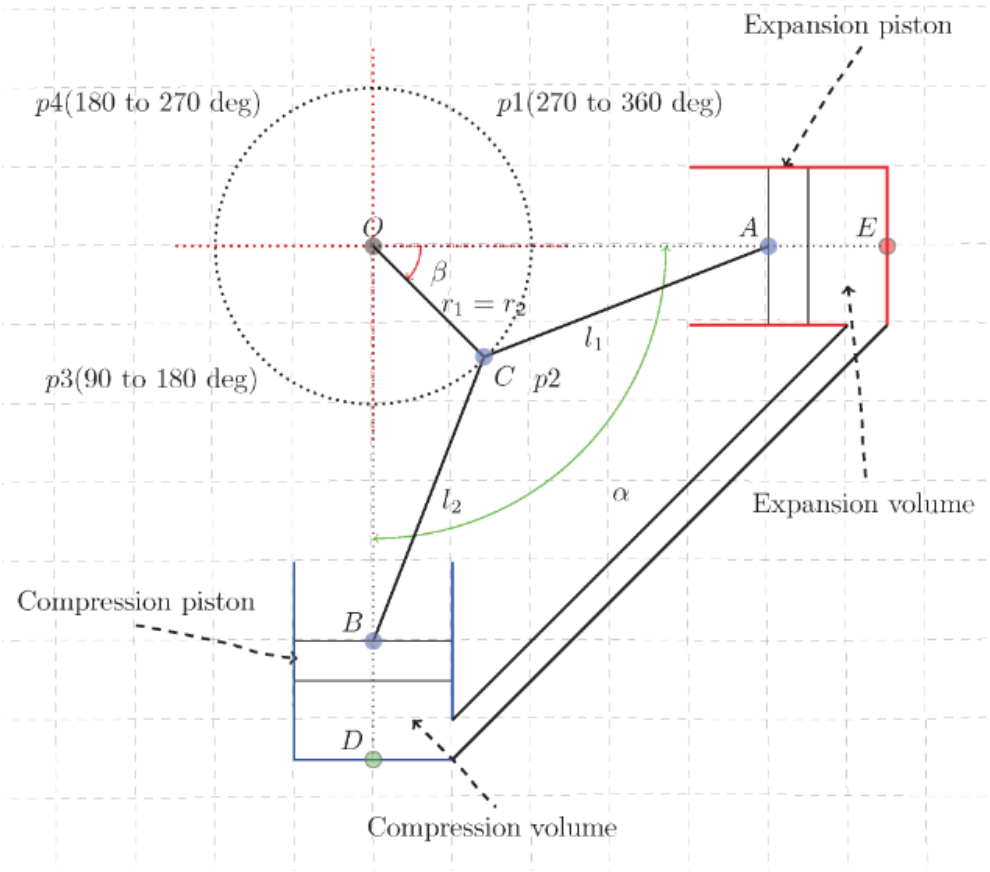

Figure 3. Schematic diagram for double slider crank [27] [Open accessed].

and other parameters are already defined above. As there is simultaneous work done by compression and expansion, due to being opposite in direction, the work done in the compression cylinder would be taken as negative. Figure 5b shows the graph of expansion volume and compression volume vs. the crank angle. Notice that both volumes are out of phase by about 90° as both the pistons are located at 90° with each other. This data is in accordance with a numerical study by [26].

$$W_{comp} = \frac{V_{se}.\pi.c.0.45.\sin a}{1+\sqrt{1-c^2}} \qquad (5)$$

$$W_{comp} = -27.739\,J$$

$$W_T = W_{exp} + W_{comp} \qquad (6)$$

$$W_T = 34.263\,J$$

Figure 3 shows the schematic diagram for the double slider crank configuration in an alpha Stirling engine. The equations for slider crank kinematics [24] are given in terms of crank radius, length, and crank angle. Successive derivatives give the equations for velocity and acceleration.

$$x = l - \frac{r^2}{4l} + r\left(\cos\Theta + \frac{r}{4l}\cos 2\Theta\right) \qquad (7)$$

$$v = -rw\left(\sin\Theta + \frac{r}{2l}\sin 2\Theta\right) \qquad (8)$$

$$a = -rw^2\left(\cos\Theta + \frac{r}{l}\cos 2\Theta\right) \qquad (9)$$

Figure 6 shows the slider crank kinematics. The acceleration, velocity and displacement are graphed to crank angle. From these kinematics calculations, balancing and vibrations are performed for the engine.

The equation for torque on the slider crank is as [24].

$$T = \frac{m_a}{2}.r^2.w^2\left(\frac{r}{2l}\sin\Theta - \sin 2\Theta - \frac{3r}{2l}\sin 3\Theta\right) \qquad (10)$$

The torque is dependent on the crank radius, length of the connecting rod, equivalent mass on the slider-crank, and the angular velocity of the crank. Solving it for 360° rotation of a crankshaft.

Figure 6 shows the forces acting on the slider crank. Notice that the forces are out of phase with each other hence cancelling most of the vibrations which is a characteristic of a 90° aligned engine. From the graph, we can notice that the

torque follows a sinusoidal waveform with alternate crests and troughs after 120°. At the start, the torque is zero as the engine starts and then it gets to a uniform speed at a given 1000 rpm for which the calculations were done.

Table 4. Regenerator without Structural Integrity and Criteria for Simulation

Quantity	Value
Max pressure	1 MPa
Factor of Safety	2
Mesh Type	Refinement Mesh + Fine Mesh
Materials	Mild Steel
Density	$7.85*10^{-6}$ kg/ mm^{-3}
Coefficient of Thermal Expansion	$1.2*10^{-5}$ C^{-1}
Specific Heat	$4.34*10^{5}$ mJ kg^{-1} C^{-1}
Thermal Conductivity	$6.05*10^{-2}$ W mm^{-1} C^{-1}
Resistivity 1.7e-004-ohm mm	$1.7*10^{-4}$ ohm mm

For a smooth power transfer, a flywheel is an integral part of an engine. The maximum stresses on the flywheel were calculated and a flywheel [24].

$$\sigma_{t_{max}} = \frac{2r}{g} w^2 \left(\frac{3+v}{8}\right)\left(r_0^2 + \left(\frac{1-v}{3+v}\right) r_i^2\right) \quad (11)$$

ANSYS Simulations and computation for material Factor of Safety and thermal and fluent analysis of the Regenerator are shown in Fig. 7

Table 4 shows data for the regenerator without structural integrity and criteria for simulation. In Figure 8, we have performed an ANSYS simulation on the regenerator. The parameters of the simulation are given in the table. We have two fixed supports and a pressure of 1 MPa applied along them, which are shaded in red. Looking at the results of the simulation we can notice that the given design has a low factor of safety. Then we added the ribs to the design, and we can see the improvement in stresses and safety in the design.

Figure 4. Stirling Engine.

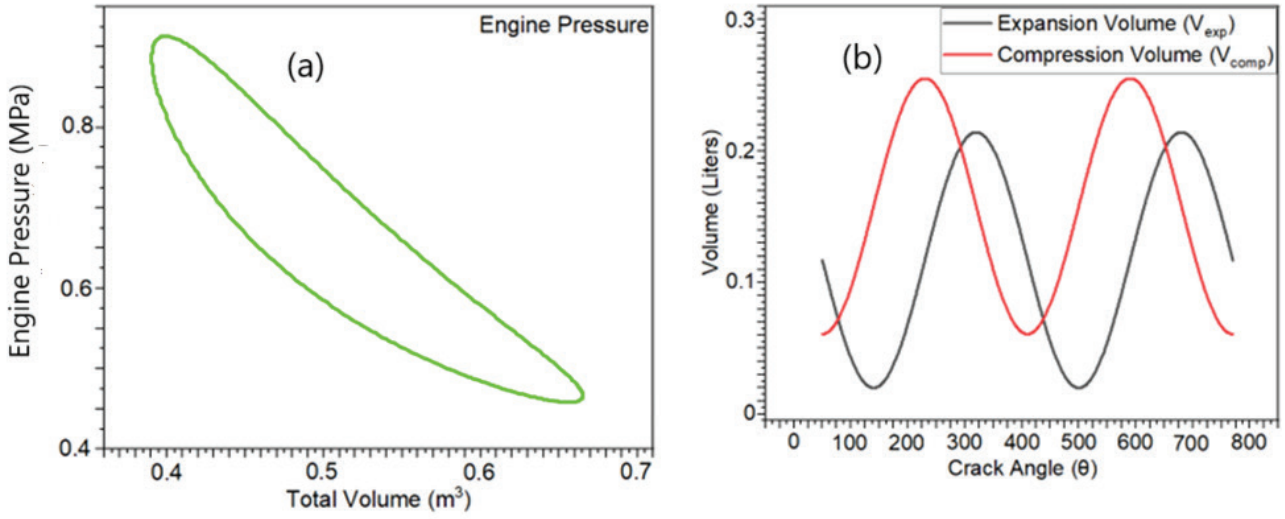

Figure 5. Characteristic Curves (a)Pressure vs Volume (b) Volume -vs-Crack Angle for α-Stirling Engine.

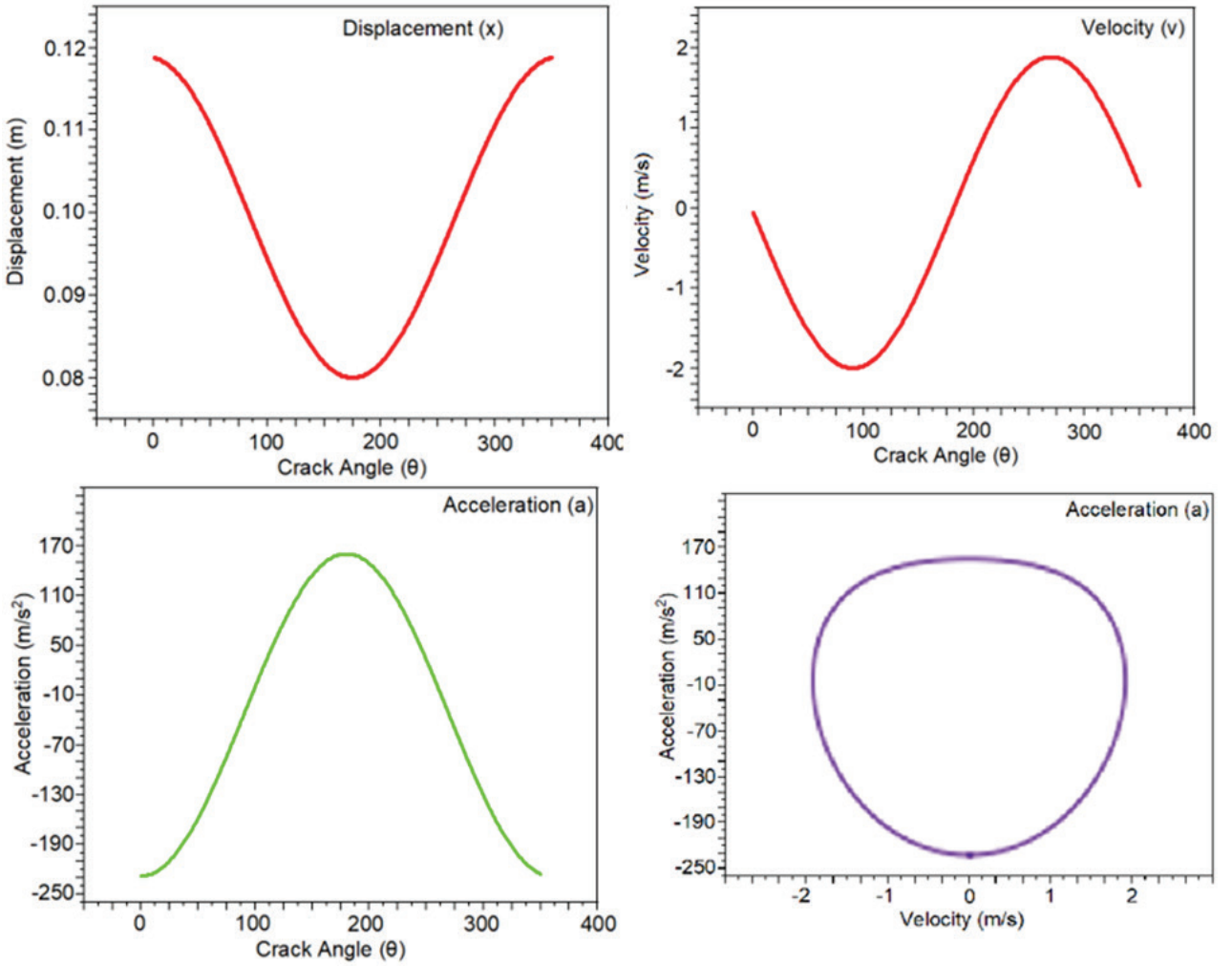

Figure 6. Slider Crank Kinematic Diagram.

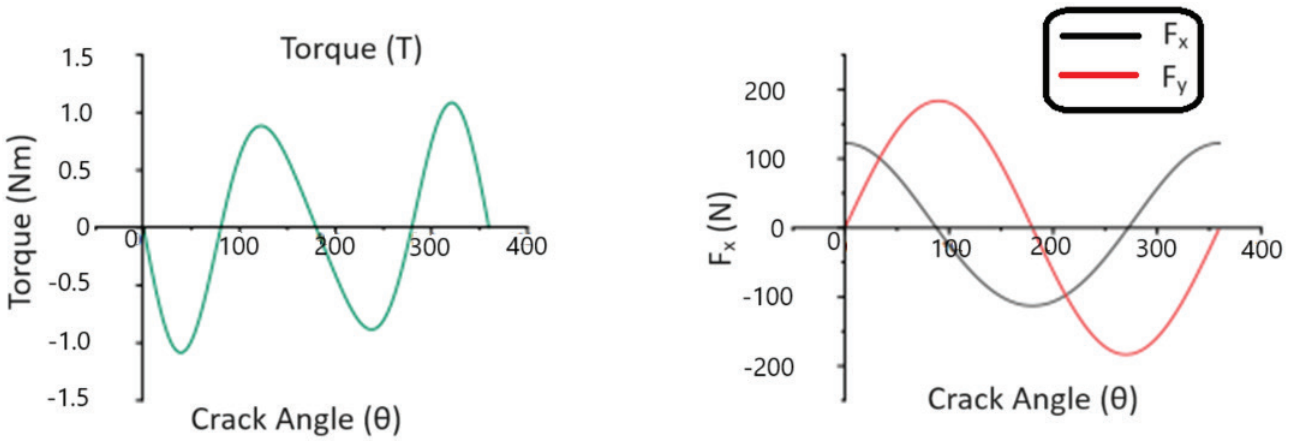

Figure 7. Torque and Force Vs Crank angle graph for Slider Crank.

In this simulation, we have made a design change while keeping other parameters constant. We can notice in Figure 9, that the strain energy is absorbed by the rib. Thus, it prevents significant deformation. The use of ribs helps us to achieve structural integrity by absorbing a definite amount of strain energy. Increasing the thickness of the wall wasn't

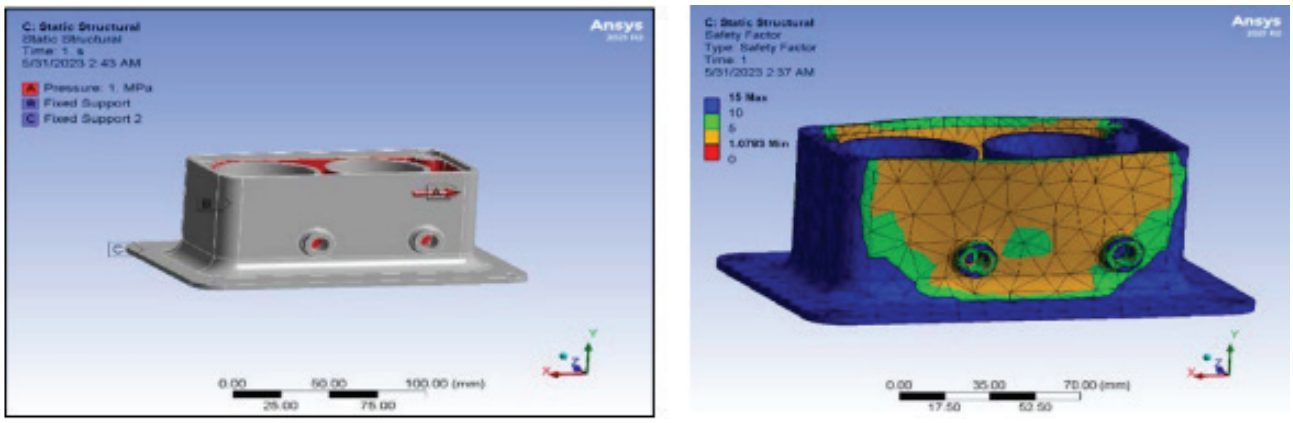

Figure 8. ANSYS Simulation for Regenerator Structural Integrity.

that effective because the strain energy was absorbed by the wall and still had a deformation. Similarly, we can also notice the increase in the factor of safety, making the design more suitable to be used under given conditions.

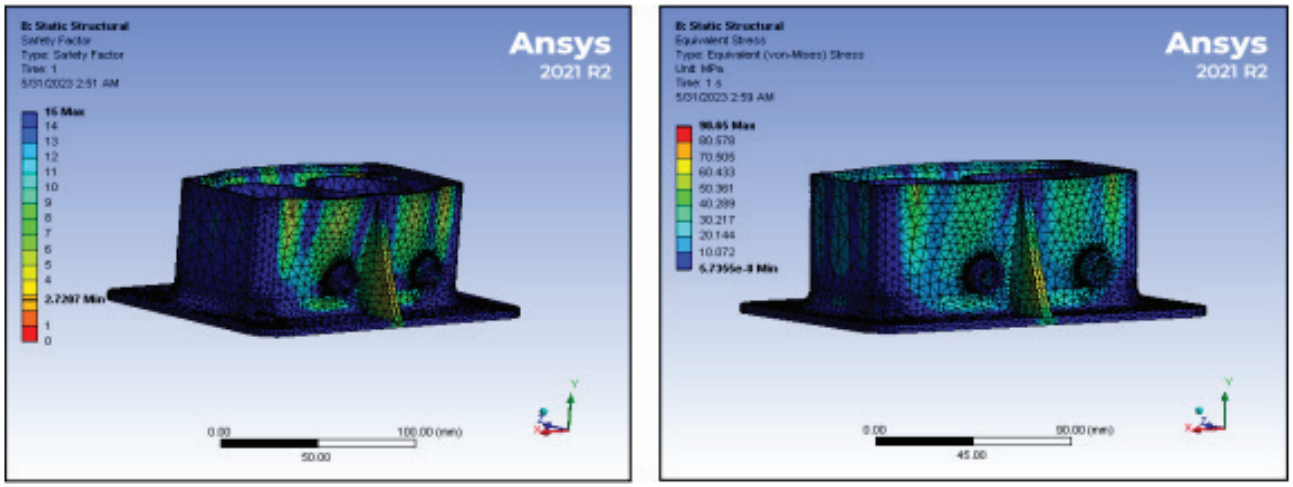

Figure 9. ANSYS Simulation for structural stability for Regenerator with ribs.

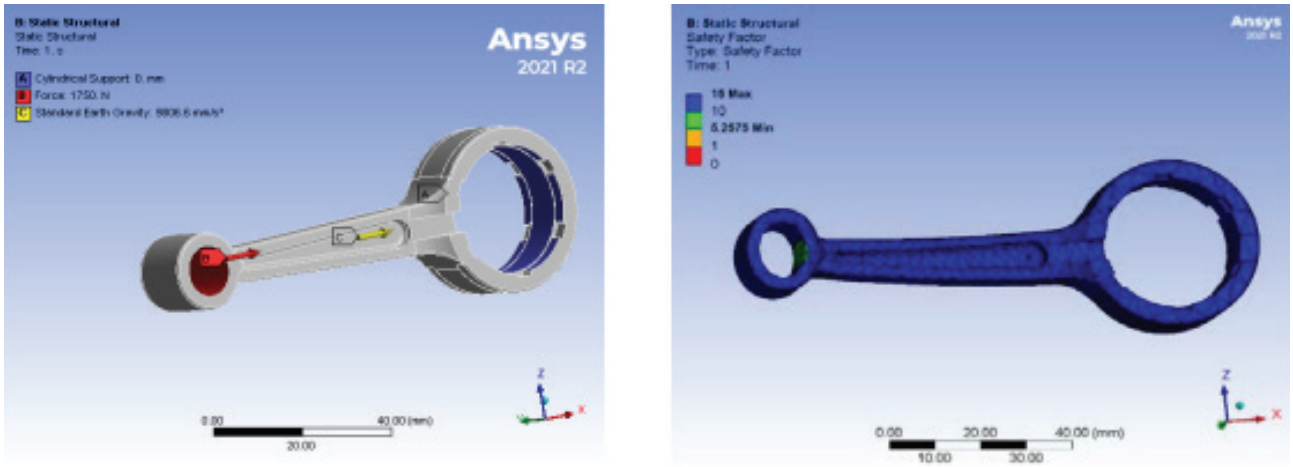

Figure 10. ANSYS Simulation Data for Connecting Rod Structural Integrity.

In figure 10, we have a connecting rod that is connected to the crankshaft and piston of the cylinder. We have performed static structural analysis for the factor of safety on it. The initial parameters include the applied force of 1750 N on face B in the figure. This force is the gas force applied on the rod by the piston. The simulation is performed with fine mesh type and we have selected the material for the connecting rod as forged steel. In the consequent figures, as the results of the simulations show, the connecting rod will withstand the applied force with an overall factor of safety on the body (colored blue) and a minimum of η= 5 factor of safety on the inside wall of the pin, which is in green color in the picture. The simulation concludes that our part will be safe during engine operation. ANSYS Simulation Data for Connecting Rod Structural Integrity is given in Table 5.

Experimental data is given in Table 6. The Solar Stirling Engine produced a power output of 77.569 wats and 523 rpm. The Schmidt analysis provides the best fit computation for the system. We have taken the engine rpm as 1000 rpm in our calculations but in actual experimentation due to mechanical losses and due to friction, we could only get around 500 rpm. That makes the deviation from computed and experimented power. The engine power has been measured it with tacheometer and dynamometer. The capacity of the system to transform solar energy into useful mechanical or electrical power is measured by thermal efficiency study. From NASA's Stirling engine design manual [28]:

$$\eta_{eff} = \left(1 - \frac{T_C}{T_H}\right) \times C \times \eta_H \times \eta_M \times f_a \qquad (12)$$

Were,

η_{eff} = overall thermal or effective efficiency

T_C, T_H = compression-expansion gas temperatures, K

C = Carnot efficiency ratio of indicated efficiency to Carnot efficiency. Calculated to be 0.68

η_H = heater efficiency, ratio between the energy flow to the heater and fuel energy flow. Calculated to be 0.86.

η_M = mechanical efficiency, ratio of indicated to brake power. Calculated to be 0.85

f_a = auxiliary ratio. At maximum efficiency point f_a= 0.95

Now Substituting Values, the average,

η_{eff} = 0.264

The energy performance matrix is given in Table 7.

The grid independence study is shown in Table 8

Table 5. ANSYS Simulation Data for Connecting Rod Structural Integrity

Quantity	Value
Length	100 mm
Max Force	750 N
Factor of Safety	2
Mesh Type	Fine Mesh
Materials	Forged Steel

Table 6. Temperature of Cylinders (Experimentally obtained)

S. No.	Max Temperature (°C) (Displacer Cylinders i.e., Hot Cylinders)	Average Temperature(°C) (Power Cylinders i.e. Cold Cylinders)
1	420	27.3
2	383	28.1
3	449	31.0
4	395	27.3

Table 7. Energy Performance Matrix

Parameter	Value (predicted)	Value (experimental)	Remarks
Thermal Efficiency	-	26.4 %	Reflects the engine's ability to convert heat into mechanical energy.
Mechanical Efficiency	-	-	Reflects internal friction and mechanical losses.
Overall Efficiency	-	26.4 %	Combined efficiency of heat conversion and mechanical work output.
Engine Speed	1000 rpm	523 rpm	Speed reduction due to mechanical losses.
Power Output	100 W	37 W	Deviation due to mechanical losses and non-ideal conditions.

Table 8. Grid Independence Study

Mesh Type	Element Size (mm)	Number of elements	Power Out Put (W)	Efficiency (%)	Remarks
Course Mesh	10	50000	35	25.2	Results show significant deviations, indicating that the mesh is too coarse.
Medium Mesh	5	150000	37	26	Results are closer to experimental data but still show minor discrepancies.
Fine Mesh	2	500000	37	26.4	Results are stable and closely match experimental data, confirming mesh independence.
Very Fine Mesh	1	1000000	37	26.4	No significant change in results, confirming that the mesh is fine enough for

As it was observed the upward trend in engine's characteristics such as power, kinematics including torque and speed etc. with respect to increase in temperature. This is in accordance with the observations in the studies by C. Yildiz et al., [29] and A. Yerbery et al., [30] who have faced similar trends in their respective research as well as the difference in predicted and actual power which was caused by manufacturing constraints as well as mechanical losses and non-ideal conditions.

EXPERIMENTAL RESULTS

The Solar Stirling Engine produced 77.569 watts at 523 RPM experimentally, deviating from the computed 1000 RPM due to friction and mechanical losses. Using NASA's Stirling engine design manual, the effective thermal efficiency was calculated to be 0.264. Efficiency factors included Carnot efficiency =0, heater efficiency =0.86, mechanical efficiency = 0.85, and auxiliary ratio = 0.95. Maximum temperatures in hot cylinders ranged from 383°C to 449°C, while cold cylinders averaged 27.3°C to 31.0°C. Increased temperature improved engine characteristics such as power, torque, and speed, consistent with prior studies.

Comparison of Results with Previous Data

Structural Analysis (ANSYS Simulation)

From the Previous Results the initial design exhibit low factor of safety, improvement were achieved by adding ribs which enhance stress distribution and wall thickness were increased with less effectiveness [27]. In current results simulations with 1 MPa pressure and mild steel properties confirmed structural challenges in the initial design, adding ribs reduced deformation by absorbing strain energy, improving safety and performance and Factors like fine mesh refinement and mild steel's thermal and mechanical properties were key to the analysis.

Thermal and Material Analysis

Previous results focused on regenerator material properties (mild steel) and its thermal performance under operating conditions. Thermal expansion, specific heat, and conductivity were used to analyze deformation and heat transfer efficiency [27]. While in current study detailed **thermal and fluent analysis** highlighted the impact of **thermal conductivity** and **coefficient of thermal expansion** on performance.

CONCLUSION

The experimental results demonstrated a power output of 37 W and an efficiency of 26.4%, compared to the predicted 100 W at 1000 rpm. However, due to mechanical losses, friction, and non-ideal operating conditions, the engine achieved a reduced speed of 523 rpm. The engine operated within a temperature range of 370–450 °C, with power, torque, and speed improving as the temperature differential between the hot and cold cylinders increased. Design constraints limited the scalability of the engine to achieve 100 W output, primarily due to market and manufacturing limitations. Mechanical losses, including flywheel inertia and friction, significantly impacted performance. To address these challenges, enhancements such as the integration of a Fresnel lens concentrator and the use of high-performance materials with superior thermal conductivity and durability were proposed. These improvements could increase compactness, efficiency, and structural integrity. The study highlights potential applications in desert and urban settings, where the engine could serve as a primary or supplementary power source for navigation aids, satellite production, and renewable energy systems. This research underscores the critical role of material selection and heat transfer optimization, paving the way for advancements in Stirling engine technology.

ACKNOWLEDGMENT

The authors greatly appreciate the support of the University of Engineering and Technology Peshawar, Pakistan

AUTHORSHIP CONTRIBUTIONS

Yasir Mehmood: conceptualization, validation, investigation, writing original draft, visualization;

Asnaf Aziz: supervision, review & editing;

Abid Hussain: Co-supervision, Data analysis;

Fasih Ur Rahman: manuscript preparation, project administration;

Afzal Khan: Review and Editing, Discussion, Validation:

Muhammad Abubakkar: manuscript preparation, discussion, review & editing;

Imad Rasool: manuscript preparation, discussion, review & editing

DATA AVAILABILITY STATEMENT

The authors confirm that the data that supports the findings of this study are available within the article. Raw data that support the finding of this study are available from the corresponding author, upon reasonable request.

CONFLICT OF INTEREST

The author declared no potential conflicts of interest with respect to the research, authorship, and/or publication of this article.

ETHICS

There are no ethical issues with the publication of this manuscript.

STATEMENT ON THE USE OF ARTIFICIAL INTELLIGENCE

Artificial intelligence was not used in the preparation of the article.

REFERENCES

[1] Butler A, Hoffman P, Smibert P, Papalexi E, Satija R. Integrating single-cell transcriptomic data across different conditions, technologies, and species. Nat Biotechnol 2018;36(5):411–420. [CrossRef]

[2] US Energy Information Administration. Frequently Asked Questions (FAQs). Much Electr Does Am Home Use 2020.

[3] Solankı A, Pal Y. A comprehensive review to study and implement solar energy in dairy industries. J Therm Eng 2021;7(5):1216–1238. [CrossRef]

[4] Kumar AR, Ramakrıshnan M. A scoping review on recent advancements in domestic applications of solar thermal systems. J Therm Eng 2022;8(3):426–444. [CrossRef]

[5] Guidi G, Violante AC, De Iuliis S. Environmental impact of electricity generation technologies: A comparison between conventional, nuclear, and renewable technologies. Energies 2023;16(23):7847. [CrossRef]

[6] Yerbury A, Coote A, Garaniya V, Yu H. Design of a solar Stirling engine for marine and offshore applications. Int J Renew Energy Technol 2016;7(1):1. [CrossRef]

[7] Asnaghi A, Ladjevardi SM, Izadkhast PS, Kashani AH. Thermodynamics performance analysis of solar Stirling engines. ISRN Renew Energy 2012;2012:1–14. [CrossRef]

[8] Nosek S, Brož K. Solar Stirling engine-the milestone of the way to meet energy demand with the lowest impact on environment. Sustain Energy Fuels 2017.

[9] Cinar C, Karabulut H. Manufacturing and testing of a gamma type Stirling engine. Renew Energy 2005;30(1):57–66. [CrossRef]

[10] Tlili I. Thermodynamic study on optimal solar Stirling engine cycle taking into account the irreversibilities effects. Energy Procedia 2012;14:584–591. [CrossRef]

[11] Gheith R, Aloui F, Nasrallah SB. Determination of adequate regenerator for a Gamma-type Stirling engine. Appl Energy 2015;139:272–280. [CrossRef]

[12] Nielsen AS, York BT, MacDonald BD. Stirling engine regenerators: How to attain over 95% regenerator effectiveness with sub-regenerators and thermal mass ratios. Appl Energy 2019;253:113557. [CrossRef]

[13] Karabulut H, Yucesu HS, Cinar C, Aksoy F. Construction and testing of a dish/Stirling solar energy unit. J Energy Inst 2009;82(4):228–232. [CrossRef]

[14] Yerbury A, Coote A, Garaniya V, Yu H. Design of a solar Stirling engine for marine and offshore applications. Int J Renew Energy Technol 2016;7(1):1. [CrossRef]

[15] Bataineh KM. Numerical thermodynamic model of alpha-type Stirling engine. Case Stud Therm Eng 2018;12:104–116. [CrossRef]

[16] Tang XY, Yang WW, Yang Y, Jiao YH, Zhang T. A design method for optimizing the secondary reflector of a parabolic trough solar concentrator to achieve uniform heat flux distribution. Energy 2021;229:120749. [CrossRef]

[17] Boretti A. Development of a hybrid concentrated solar-natural gas system. Int J Energy Res 2021;45(11):17015–17021. [CrossRef]

[18] Kayofa L. Feasibility Study and Business Plan for Manufacturing a 3 kW-Electrical Solar Stirling Engine and Dish for Stand-Alone Power Supply Units [PhD thesis]. Stellenbosch: Stellenbosch University; 2015.

[19] López-Castrillón W, Sepúlveda HH, Mattar C. Off-grid hybrid electrical generation systems in remote communities: Trends and characteristics in sustainability solutions. Sustainability 2021;13(11):5856. [CrossRef]

[20] Zhu S, Yu G, Liang K, Dai W, Luo E. A review of Stirling-engine-based combined heat and power technology. Appl Energy 2021;294:116965. [CrossRef]

[21] Alipour N, Jafari B, Hosseinzadeh K. Analysis of the impact of metal foam with phase change material on solar photovoltaic thermal system efficiency. J Energy Storage 2024;98:113064. [CrossRef]

[22] Aigboviosa AP, Anthony A, Claudius A, Uzairue S, Timilehin S, Imafidon V, et al. Arduino based solar tracking system for energy improvement of PV solar panel. In: Proceedings of the International Conference on Industrial Engineering and Operations Management; 2018. p. 2469–2478.

[23] Thombare DG, Verma SK. Technological development in the Stirling cycle engines. Renew Sustain Energy Rev 2008;12(1):1–38. [CrossRef]

[24] Tanaka C, Kamata H, Takeshita H, Yagisawa H, Hirata H. Redox regulation of lipopolysaccharide (LPS)-induced interleukin-8 (IL-8) gene expression mediated by NFκB and AP-1 in human astrocytoma U373 cells. Biochem Biophys Res Commun 1997;232(2):568–573. [CrossRef]

[25] Lam N, Tuner M, Tunestal P, Andersson A, Lundgren S, Johansson B. Double compression expansion engine concepts: A path to high efficiency. SAE Int J Engines 2015;8(4):1562–1578. [CrossRef]

[26] Bataineh K. Mathematical formulation of alpha-type Stirling engine with Ross Yoke mechanism. Energy 2018;164:1178–1199. [CrossRef]

[27] Egas J, Clucas DM. Stirling engine configuration selection. Energies 2018;11(3):584. [CrossRef]

[28] Martini WR. Stirling Engine Design Manual. NASA; 1983.

[29] Yildiz C, Bayata F, Mugan A. Multi-objective optimum design of an alpha type Stirling engine using meta-models and co-simulation approach. Energy Convers Manag 2021;232:113878. [CrossRef]

[30] Yerbury A, Coote A, Garaniya V, Yu H. Design of a solar Stirling engine for marine and offshore applications. Int J Renew Energy Technol 2016;7(1):1. [CrossRef]